communications earth & environment

Article

https://doi.org/10.1038/s43247-024-01483-8

Tidal and seasonal influence on cold seep activity and methanotroph efficiency in the North Sea

Tim R. de Groot[1] ✉, Malika Menoud[2], Judith van Bleijswijk[1], Sonja M. van Leeuwen[1], J. van der Molen[1], Victor Hernando-Morales[1,3], Helen Czerski[4], Hossein Maazallahi[2], Sylvia Walter[2], Darci Rush[1], Thomas Röckmann[2] & Helge Niemann[1,5,6] ✉

The ocean's methane emission to the atmosphere is dominated by continental shelves where cold seeps are globally common features. Seeps emit methane into the hydrosphere, but temporal variations and controls of seep activity and the efficiency of the microbial methane filter in the water column are scarce. Here we address these knowledge gaps by measuring whole water column methane inventories and methanotrophic activity at a temporal resolution of 2 hours at a North Sea cold seep (Doggerbank) in summer and autumn. We found that bottom water methane inventories were 68% (summer) and 11% (autumn) higher during low tide compared to high tide coinciding with increased methanotrophic activity. The activity of methanotrophs was reduced during autumn when the water column was fully mixed and matched by higher methane emissions to the atmosphere. Our results show that tides are underappreciated controls on seepage and methanotrophic activity and methane sea–atmosphere fluxes.

Methane (CH_4) is an important greenhouse gas, which is 32 times more potent than CO_2 (averaged over a time horizon of 100 years)[1]. Though the half-life of atmospheric CH_4 is relatively short (~9 years), CH_4 concentrations in the atmosphere have risen drastically to current values of ~1.9 ppm; ~2.5-fold higher than preindustrial concentrations[2]. The exact mechanisms behind this increase are not fully understood, yet it is clear that it is predominantly caused by anthropogenic emissions[3]. The source strengths of these are fairly well constrained (336–376 Tg yr^{-1}) but large uncertainty exists about the strength of individual natural sources, which together contribute about 40% (183–248 Tg yr^{-1}) to the total atmospheric budget[2,4]. Shelf seas are the main contributor of total oceanic CH_4 emission to the atmosphere (9–22 Tg yr^{-1}), although they only account for 8−10% of the global ocean surface[4,5].

Compared to the open ocean, shelf seas are characterised by high nutrient loads, high primary production, high sedimentation rates, and subsequent burial of dead organic matter to the seabed. This leads to elevated CH_4 production in sediments mediated by microbial or thermogenic processes[6,7]. At cold seeps, CH_4 migrates upwards through cracks and fissures in the sea bed and may be released as dissolved or free gas into the water column[8]. Cold seeps are thus CH_4 hotspot point sources, and they occur frequently along shelf seas across the globe[9,10], promoting CH_4 transport to the atmosphere[11,12]. Nevertheless, a substantial amount of the water column CH_4 content is consumed by aerobic methane oxidising bacteria (MOB) that mediate the aerobic oxidation of methane (MOx)[6]:

$$CH_4 + 2O_2 \rightarrow CO_2 + 2H_2O \quad (1)$$

In the water column, MOB thus form a microbial CH_4 filter, that acts as a sink for CH_4 before it reaches the atmosphere[7,13,14]. The known MOB comprise Gammaproteobacteria (type I and type X), Alphaproteobacteria (type II), Verrucomicrobia, and members of candidate division NC10[15]. Similar to other metabolic processes involving small molecules, MOx removes isotopically light CH_4 so that the residual CH_4 pool successively becomes ^{13}C and ^{2}H (D) enriched[16,17]. Methanotrophic activity in the water column is determined by the availability of CH_4, oxygen, and nutrients[6,18], and, importantly, the continuity of environmental conditions[8,9,14]. While shelf seas are typically rich in CH_4, O_2, and nutrients, continuity is disrupted by the extremely dynamic nature of the coastal ocean. On daily time scales, tides induce changes in hydrostatic pressure and currents, and they also

[1]NIOZ Royal Netherlands Institute for Sea Research, Texel, Netherlands. [2]Institute for Marine and Atmospheric (IMAU) Research, Utrecht University, Utrecht, Netherlands. [3]Centro de Investigación Mariña (CIM), University of Vigo, Vigo, Spain. [4]Department of Mechanical Engineering, University College London, London, United Kingdom. [5]Department of Earth Sciences, Utrecht University, Utrecht, Netherlands. [6]CAGE—Centre of Arctic Gas Hydrate, Environment and Climate, Department of Geosciences, UiT the Arctic University of Norway, Tromsø, Norway. ✉e-mail: tim.de.groot@nioz.nl; helge.niemann@nioz.nl

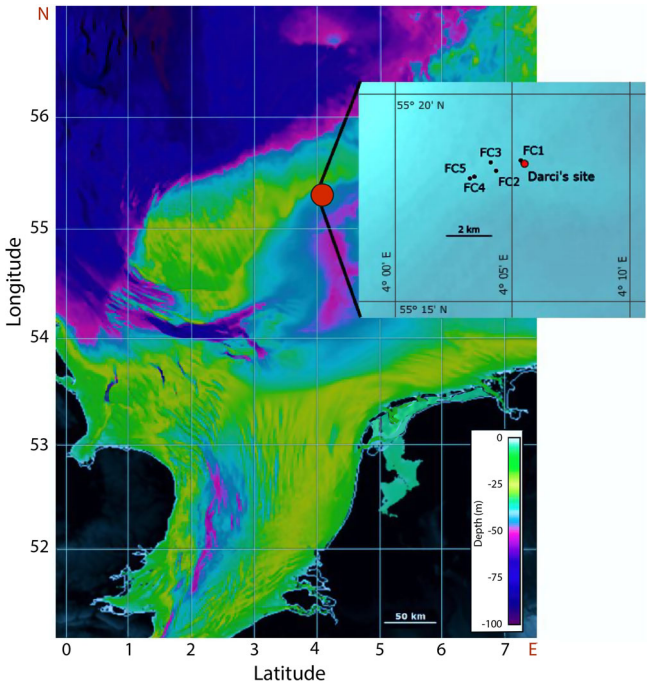

Fig. 1 | Bathymetry of the Doggerbank area. The sectional enlargement shows the position of Darci's site. Previously determined locations for flare clusters (FC) are marked[25,26].

exert force on the solid geosphere[19]. On seasonal time scales, mixing regimes shift as a result of temperature changes and wind forcing[20,21].

In shallow waters such as those encountered on the shelf, the distance separating CH_4 liberation from the sea floor and CH_4 emission to the atmosphere is small so that the time for water column CH_4 consumption is limited; changes in environmental conditions are thus likely to strongly effect water column CH_4 dynamics[8,13,21,22]. Nevertheless, most investigations in the field lack temporal replication and have been conducted during fair weather conditions. Thus, our knowledge of seepage and seep-associated biogeochemical processes typically covers only distinct snapshots in time. Little qualitative and/or quantitative knowledge exists regarding the effect of tidally[23–26] and seasonally induced[14,27,28] changes on cold seep dynamics and the efficiency of the microbial CH_4 filter in the water column. This is reflected in the large uncertainty of the contribution of coastal waters to the atmospheric CH_4 budget[4,5].

In this study, we conducted high-frequency time-series measurements at a fixed position at an active cold seep (41 m water depth, Doggerbank seep area in the Southern North Sea) in summer and late autumn. We found that tides apparently modulated seepage activity, which, together with water column mixing, controlled the capacity of the microbial water column CH_4 filter. These variations had profound effects on CH_4 emissions to the atmosphere.

Results

We visited a shallow water cold seep area at the south-eastern flank of the Doggerbank in the North Sea (Fig. 1) during stratified (summer; June/July 2018) and well-mixed water column conditions (autumn; Oct. 2019). During both expeditions, we documented multiple clusters of acoustic flares caused by CH_4 bubbles emanating from the seafloor and we visually observed bubbles breaking through the sea surface. The position of the flare cluster investigated here in more detail (hereafter termed 'Darci's site') was slightly offset (~45 m to the southeast) compared to previous reports[29,30]. We cannot determine if this is related to a geographical shift of CH_4 conduits and exit points at the seafloor or due to the instrumental or graphical resolution of the previous reports. We recorded positions with a differential GPS system and corrected for the spatial difference between the GPS antenna, multibeam transducer, and the actual CTD cast position. All CTD measurements at Darci's site were taken directly over the several hundred to thousand m^2 area where bubbles were rising from the sea floor[30]. We continuously monitored water column CH_4 dynamics over a ~2-day period, both during stratified and mixed conditions (29 June - 1 July 2018 and 12 October - 14 October 2019). Our aim was to unravel potential temporal effects (diurnal) on water column methane dynamics related to variations in seep activity or seasonal mixing (variations in water column CH_4 concentrations) and the capacity of the microbial CH_4 filter (activity of methanotrophs in the water column). It has to be noted that the limited duration of our study may impose constraints on fully resolving the complexity of the seep system and the effects of tides and seasonality.

Water column properties

During the summer campaign, the water column was highly stratified throughout the entire period of investigation with a pycnocline located at about 25 m water depth (with slight variations related to tidal phase, Supplementary Fig. 1). Hereafter, waters below the pycnocline are referred to as bottom waters and waters above the pycnocline are referred to as surface waters. Temperature changed from 14.7 °C in surface waters to 7.2 °C in bottom waters and was the main driver for density stratification because salinity was relatively constant at ~34.78 psu. In contrast to summertime, the water column was fully mixed in late autumn (Supplementary Fig. 1). Water temperature and salinity were uniform throughout the time series with average values of ~14 °C and ~34.76 psu, respectively.

Water column methane dynamics

In summer and in autumn, dissolved CH_4 concentrations were highly variable, both on a vertical and a temporal scale Fig. 2E, F). Nevertheless, clear patterns were apparent: during both seasons, we found temporally reoccurring maxima and minima in CH_4 concentrations, markedly in bottom waters, that roughly followed a 12-hour periodicity matching tidal oscillation. Independent of season, we often found highest CH_4 concentrations around low tide and lowest concentrations around high tide (Fig. 2K, L). Specifically in bottom waters during summertime, CH_4 concentrations at low tide (min = 11 nM, max = 2082 nM) were higher than during high tide (min = 14 nM, max = 838 nM). For statistical comparison, low and high tide times are defined as the actual low tide or high tide time ±2 h. These difference translated to a significant ($p \leq 0.01$, Welch's t-test, supplementary Table 1) difference of ~3.3-fold on average in the bottom water CH_4 concentrations when comparing low and high tide (Table 1) with generally higher concentrations during low tide ±2 h (average = 477 nM) compared to high tide ± 2 h (average = 146 nM). Furthermore, Summer CH_4 concentrations were significantly higher in bottom waters (average = 266 nM bottom waters vs. 61 nM in surface waters, $p \leq 0.001$, Welch's t test, supplementary Table 2). The differences in CH_4 concentrations translate to similar differences in CH_4 inventories (Table 1). CH_4 concentrations during low tide compared to high tide were also elevated in autumn, however, these differences were not statistically significant (Table 1, supplementary Table 1).

Besides temporal changes on a diel scale, we also found seasonal differences in water column CH_4 concentrations, which were higher in summer (average = 137 nM), compared to autumn (average = 52 nM). These differences were significant, both in surface waters ($p \leq 0.03$; Welsch's t test) and bottom waters ($p \leq 0.001$, Supplementary Table 3) and translated to a ~2-fold lower methane inventory in autumn compared to summer (Table 1).

Visually, we could observe bubbles breaking the sea surface during both seasons. We investigated the size of these bubbles in situ with a custom-built ocean bubble camera at 2 m water depth in autumn[31]. These measurements revealed an average bubble radius of 0.73 ± 0.49 mm (Supplementary Fig. 2, Supplementary Table 4).

Sea surface-atmosphere methane fluxes

Sea surface-atmosphere CH_4 fluxes were calculated from the seawater–atmosphere CH_4 gradient, and wind speed. CH_4 concentrations in the well-mixed surface layer varied between 1.5 and 139 nM (Fig. 2C, D) and between 1.87 and 2.12 ppm in the atmosphere (Fig. 2A, B). Wind speed

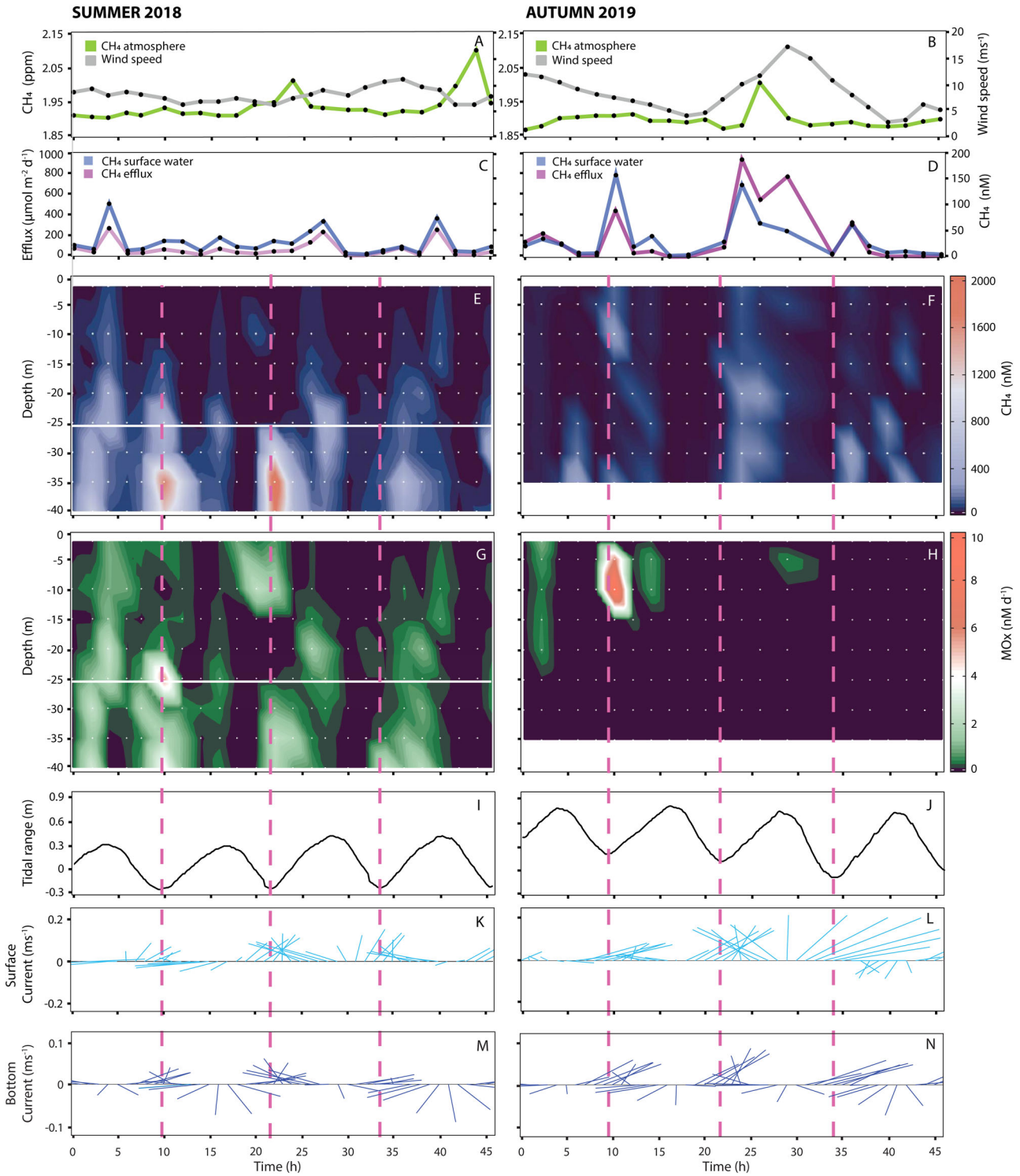

Fig. 2 | Methane dynamics at Darci's site. Seasonal methane concentrations in the atmosphere (10 m above sea surface) and local wind speed (**A**, **B**). Diffusive flux of methane at the sea surface and methane concentration in well-mixed surface waters (**C**, **D**). Spatiotemporal distribution of methane concentration (**E**, **F**), aerobic methane oxidation (**G**, **H**), tidal range (**I**, **J**), surface current direction and velocity (**K**, **L**), and bottom current direction and velocity (**M**, **N**). The sampling time series started at 13:30 h on 29 June 2018 and at 11:30 h on 12 October 2019). White dots denote actual sampling depth/time. The pycnocline (only present in summertime) is depicted as a white horizontal line (**E**, **G**). Vertical pink dotted lines indicate low tide.

was higher in autumn (average = 8 m s^{-1}, max = 17 m s^{-1}) compared to summertime (average = 7 m s^{-1}, max = 9.5 m s^{-1}). During both campaigns (with one exception in summer and two in autumn), we found positive CH_4 emissions to the atmosphere (Fig. 2A, G). However, CH_4 efflux was 2.8-fold lower in summer during stratified conditions (average = 64 μmol m^{-2} d^{-1}, max = 265 μmol m^{-2} d^{-1}) compared to autumn when the water column was fully mixed (average = 180 μmol m^{-2} d^{-1}, max = 935 μmol m^{-2} d^{-1}, Table 1).

Aerobic methane oxidation

Similar to water column CH_4 concentrations, methane oxidation rates were highly variable, but roughly followed a ~12-hour periodicity. Specifically,

Table 1 | Methane dynamics at Darci's site

	Summer 2018	Autumn 2019
Stratified waters	Yes	No
Volumetric averages		
Methane (nmol L^{-1})		
Surface water (2 m)	26 ± 24	*33 ± 42*
Surface waters (2 m–25 m)	61 ± 86	*40 ± 61*
Bottom waters (25 m–40 m)	266 ± 409	*88 ± 118*
Water column	137 ± 277	52 ± 81
Surface water LT ± 2 h	52 ± 58	55 ± 75
Bottom water LT ± 2 h	477 ± 585	108 ± 130
Surface water HT ± 2 h	70 ± 92	29 ± 41
Bottom water HT ± 2 h	146 ± 159	87 ± 124
MOx (nmol $^{-1}$ d^{-1})		
Surface waters (2 m–25 m)	0.38 ± 0.68	*0.17 ± 1.03*
Bottom waters (25 m–40 m)	0.64 ± 0.86	*0.002 ± 0.01*
Water column	0.48 ± 0.76	0.13 ± 0.89
Surface water LT ± 2 h	0.42 ± 0.91	*0.35 ± 1.70*
Bottom water LT ± 2 h	1.1 ± 1.02	*0 ± 0*
Surface water HT ± 2 h	0.41 ± 0.52	*0.09 ± 0.22*
Bottom water HT ± 2 h	0.48 ± 0.72	*0.001 ± 0.005*
Methane sea–air flux		
CH_4 flux (μmol m^{-2} d^{-1})	64 ± 77	180 ± 272
Areal inventories		
Methane (μmol m^{-3})		
Surface waters (0 m–25 m)	1282 ± 1078	*1003 ± 1098*
Bottom waters (25 m–40 m)	3535 ± 4694	*1264 ± 1410*
Total water column	4817 ± 5024	2267 ± 2173
Surface water LT ± 2 h	1080 ± 828	1430 ± 1460
Bottom water LT ± 2 h	6034 ± 6793	1465 ± 1622
Surface water HT ± 2 h	1510 ± 1322	883 ± 847
Bottom water HT ± 2 h	2119 ± 1950	1303 ± 1462
MOx (μmol m^{-2} d^{-1})		
Surface waters (0 m–25 m)	8.5 ± 8.1	*4.6 ± 16.1*
Bottom waters (25 m - 40 m)	9.1 ± 10	*0.1 ± 0.1*
Total water column	17.7 ± 14.8	4.7 ± 16.1
Surface water LT ± 2 h	9.5 ± 7.7	9.7 ± 26.5
Bottom water LT ± 2 h	14.4 ± 11	0.0 ± 0.0
Surface water HT ± 2 h	9.0 ± 9.3	2.1 ± 4.3
Bottom water HT ± 2 h	7.0 ± 8.7	0.0 ± 0.1

Methane concentrations and MOx were averaged over depth (summer 40 m and autumn 35 m), and the inventories of methane and MOx were computed by integrating values over a depth interval of 40 m in both seasons. The data for methane and MOx were averaged over the entire time series. Methane and MOx for low tide (LT) and high tide (HT) were averaged over a 4 h time period across the actual low and high tide, i.e. ±2 h. It should be noted that no distinct surface and bottom water masses were present during fully mixed conditions (autumn). Therefore, the individual autumn inventories of methane and MOx are presented in italic font for comparative purposes only. The average wind speed during the sampling period was 7.0 (±1.14) and 8.4 (±3.66) m s^{-1} in summer and autumn, respectively.

during stratified conditions, MOx was significantly higher during low tide compared to high tide ±2 h ($p \leq 0.02$, Welsh's t test; Fig. 2I–J and Supplementary Table 1). Additionally, the first order rate constant, k, was elevated during low tide, too (Supplementary Fig. 3). This feature was most prominent in summer below the pycnocline. However, elevated MOx was also observed above the pycnocline, e.g., at 10 m water depth after 20 hours during the summer campaign. Thus, stratification did not limit MOx to bottom waters; in fact, we found similar averages of depth-integrated MOx rates above (8.5 ± 8.1 μmol m^{-2} d^{-1}) and below (9.1 ± 10 μmol m^{-2} d^{-1}) the pycnocline (Table 1). In contrast to the summer season, MOx was lower in autumn both in bottom waters ($p \leq 0.001$, Welsh's t test) and surface waters ($p \leq 0.06$, Supplementary Table 3). Notably, individual MOx measurements were typically lower in autumn (with one exception: after 10 hours of investigation, MOx was 6 nM d^{-1} at 5 m, and 10 nM d^{-1} at 10 m water depth, which was higher than the maximum MOx in summer).

Carbon and hydrogen isotope systematics

Samples with high CH_4 concentrations most likely reflect isotopically unaltered CH_4 emitted from the sea floor. This is supported by the fact that the isotopic composition at high CH_4 concentrations (i.e., >200 nM in summer and autumn) was relatively uniform with values of -82 ± 0.5‰ ($\delta^{13}C$-CH_4) and −189 ± 3‰ (δD-CH_4) in summer and $\delta^{13}C$-CH_4 = −80 ± 1.3‰, δD-CH_4 = −189 ± 2.4‰ in autumn. These values are typical for a microbial (carbonate reduction) origin of CH_4[16,32]. At low tide, i.e., during times of higher CH_4 concentrations, we found that the $\delta^{13}C$-CH_4 and δD-CH_4 source signal was generally conserved throughout the water column. At high tide, i.e., during times of lower CH_4 concentrations, $\delta^{13}C$ and δD signatures of CH_4 were heavier (Supplementary Fig. 4). For example, after a period of reduced seepage in summer after 16 hours (Fig. 2E), the isotopic signal of CH_4 in bottom waters shifted from −80‰ to values of about −69‰ ($\delta^{13}C$) after 18 hours, before shifting back to −80‰, 4 hours later at a time when seep activity increased leading to higher CH_4 concentrations. However, a periodicity as found for CH_4 concentrations and MOx rates was less visible in the $\delta^{13}C$-CH_4 and δD-CH_4 values.

We used a two-endmember mixing model[33,34] and a Rayleigh fractionation model to investigate if the enrichment of the residual CH_4 in heavy isotopes (i.e. ^{13}C and D) was caused by MOx, which is known to discriminate against heavy isotopes[16,17], or by mixing with comparably heavy atmospheric CH_4 ($\delta^{13}C$ and δD of atmospheric CH_4 = ca. −47‰ and ca. −85‰, respectively[35]). The two endmembers were (i) well-mixed surface waters in equilibrium with atmospheric methane and (ii) the maximum CH_4 concentration in bottom waters, both with their respectively associated isotopic signature. Linear mixing alone would result in concentration/isotope data as depicted by the mixing lines in Fig. 3. For the lower concentrations, our results show clear deviations from this mixing line. At CH_4 concentrations <60 nM, the co-variation of CH_4 concentration and isotope values for many samples was consistent with Rayleigh fractionation processes (Fig. 3 and Supplementary Fig. 5), providing evidence for the removal of isotopically light CH_4 from the water column as is typical for ongoing MOx.

Community of MOB

Analysis of 16 S rRNA gene amplicon sequencing showed that the relative abundance of known MOB genera was rather low, comprising <0.01% and <0.02% of total bacterial reads in the water column in summer and autumn, respectively (Fig. 4; note that no known methanotrophs could be detected in summertime surface waters using amplicon sequencing). During both sampling campaigns, the genus Methyloceanibacter of the family Methyloligellaceae was the most dominant potential methanotroph in the water column (>92% of total MOB reads). This genus is known to contain designated type II methanotrophs[36], suggesting that it plays a key role at Darci's site (note that this genus also contains species of methylotrophs that metabolise C_1-compounds other than CH_4[36], see also discussion in section 'factors controlling methane oxidation'). Other MOBs detected in in the water column belong to the family Methylomonadaceae, most importantly the genera pltb-vmat-59, and pLW−20. In addition to MOBs, we also observed relatively high abundances of members of the OM43 clade within the family Methylophilaceae (0.25% and 0.27% of total bacterial reads, in summer and in autumn, respectively, data not shown). The OM43 clade comprises methylotrophs that most likely cannot oxidise CH_4 directly, but may benefit from methanol, which is produced as an intermediate during MOx[37]. Methanotroph-methylotroph associations are currently not well constrained and are a subject of ongoing research[37–39].

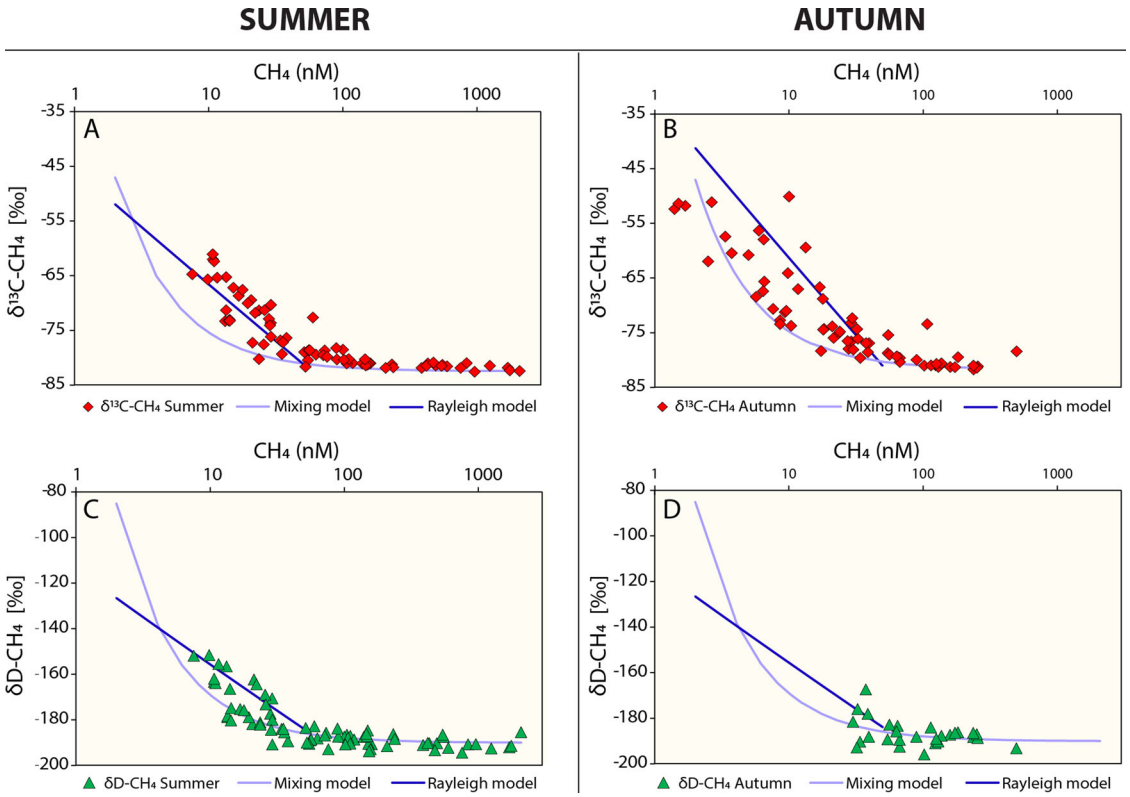

Fig. 3 | Methane stable isotope composition and concentration–mixing and oxidative removal. CH_4 concentration versus stable carbon isotope composition in summer (**A**) and autumn (**B**), and stable hydrogen isotope composition in summer (**C**) and autumn (**D**). Purple lines show results of a two-endmember mixing model with well-mixed ocean surface waters, and CH_4 charged bottom waters as end-members. CH_4 stable isotope composition and concentration following oxidative removal according to the Rayleigh model are depicted as a blue line, using the low-concentration end of the stable isotope distribution as a starting point for the model. ε values for carbon (ε_C summer: −7.8‰ and ε_C autumn: −7.5‰) and hydrogen (ε_H summer: −15.9‰) isotopes were determined from CH_4 data at concentrations <60 nM (Supplementary Fig. 5). The mixing model is not well constrained for δD-CH_4 in autumn, the curve is only shown for comparison.

In top layer sediments, the relative MOB abundance (up to 0.44% and 0.12% of total bacterial reads in summer and autumn, respectively), as well as the diversity of known methanotrophic families, was higher than in the water column (Fig. 4). MOB in top sediments were dominated by the potential type II MOB Methyloceanibacter (41% of MOB reads in summer and 62% of MOB reads in autumn). Furthermore, we also found sequences belonging to the type I MOB Methyloprofundus (23% and 7% of MOB reads in summer and autumn) as well as Crenothrix (5% of MOB reads in summer), lheB2-23 (8% and 7% of MOB reads in summer and autumn, respectively), Marine Methylotrophic Group 2 (7% and 6% of MOB reads in summer and autumn, respectively), pLW-20 (6% and 1% of MOB reads in summer and autumn, respectively), and pltb-vmat-59 (2% and 8% of MOB reads in summer and autumn, respectively).

Absolute abundance of Methyloceanibacter, Methyloprofundus, and OM43 clade

qPCR analysis showed contrasting trends in absolute abundance of Methyloceanibacter, Methyloprofundus, and OM43 copy numbers when comparing the water column with sediments (Fig. 5). With qPCR, we were also able to detect Methyloceanibacter in surface waters in summer, which was not detectable using less sensitive amplicon sequencing (Fig. 4). This observation underscores the need for employing complementary methodologies in microbial community studies to capture the complete spectrum of microbial diversity and abundance. In summer, the absolute abundance of Methyloceanibacter 16 S gene copies were sixfold higher in bottom waters (Fig. 5; average = 460; max = 809 copies mL^{-1}) than surface waters (average = 73; max = 467 copies mL^{-1}). Methyloceanibacter was less abundant at the reference station, yet we found a similar trend with higher copy numbers in bottom (379 copies mL^{-1}) than surface waters (89 copies mL^{-1}). In sediments, Methyloceanibacter were highly abundant (average = 6.9×10^6; max = 7.5×10^6 copies g^{-1}) suggesting that sediments could function as a source for Methyloceanibacter in the water column. A more contrasting water column-sediment trend was found for Methyloprofundus (Fig. 5): the abundance of this MOB was low in bottom waters (average = 20; max = 81 copies mL^{-1}), but an order of magnitude higher than Methyloceanibacter in top sediment layers (average = 2.2×10^7, max = 2.8×10^7 copies g^{-1}). On the other hand, copy numbers of the OM43 clade were highly abundant in both, surface (average = 3.1×10^4, max = 6.1×10^4 copies mL^{-1}) and bottom waters (average = 2.6×10^4, max = 9.3×10^4 copies mL^{-1}). Copy numbers of the OM43 clade in sediments (average = 6.1×10^5, max = 1.1×10^6 copies mL^{-1}) were >1 order of magnitude lower compared to Methyloceanibacter and Methyloprofundus.

In autumn, 16S gene copies of Methyloceanibacter and the OM43 clade were higher compared to summertime conditions (1.2 and 1.6-fold, respectively, in bottom waters; 5 and 1.6-fold, respectively in surface waters). Top layer sediment contained a similar amount of Methyloceanibacter 16 S gene copies (average = 9.3×10^6, max = 1.3×10^7 copies g^{-1}) when compared to summertime, while the OM43 clade was 8-fold less abundant in sediments in autumn compared to summer. In autumn, Methyloprofundus could not be detected in the water column and was also 20 times lower in abundance in sediments.

Discussion

The maximum CH_4 concentration in the water column at Darci's site (2028 nM) is comparable to other highly active seeps and gassy sediments releasing CH_4 to the hydrosphere[8,28,40,41]. Natural gas release from seafloor sediments to the hydrosphere is globally common on continental margins[5,9,28]. Yet, the flux from continental margins to the atmosphere is

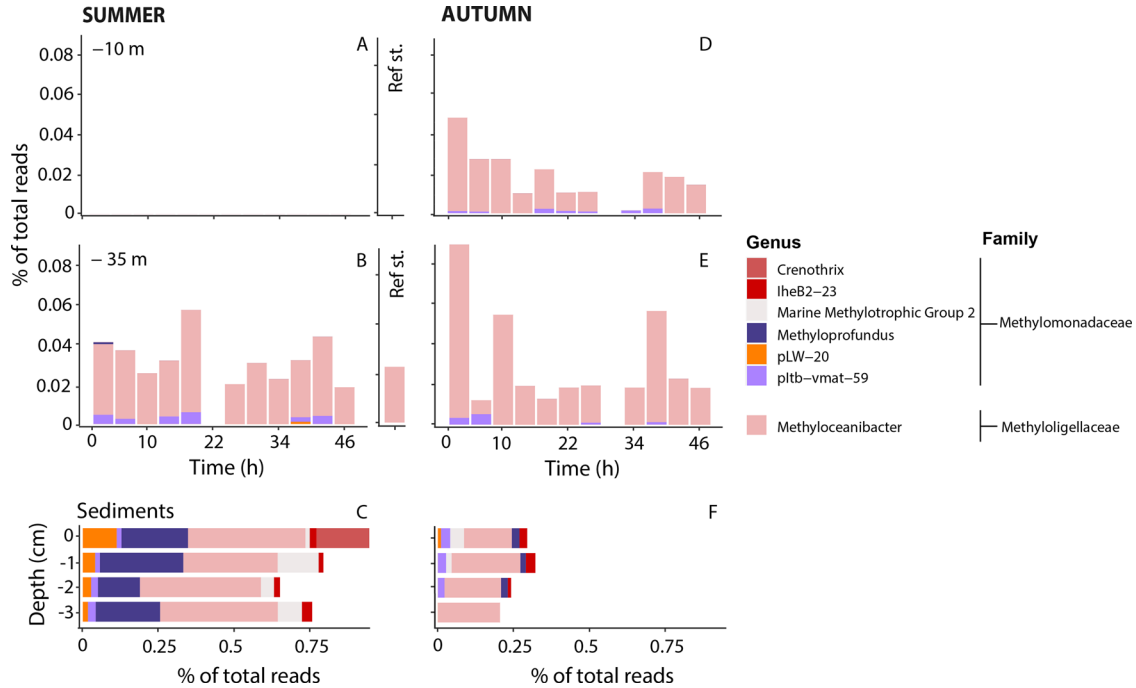

Fig. 4 | Diversity of aerobic methane oxidising bacteria. Relative abundance of 16S rRNA gene reads of families of known and potential MOBs in the water column (**A**–**D**) and sediments (**E**, **F**). Note that the genus Methyloceanibacter also contains methylotrophs that utilise C_1-compounds other than methane. No known methanotrophs could be detected in surface waters in summertime. No samples were recovered at 20 hours in summer and 32 hours in autumn and at the reference station in autumn due to bad weather. The summer reference station is located 35 km NNW from Darci's site.

Fig. 5 | Quantitative abundance of aerobic methane oxidising bacteria. Spatiotemporal abundance was determined with qPCR for Methyloprofundus, Methyloceanibacter, and Methylotrophic genera OM43 Clade in the water column (**A**–**D**) and in sediments (**E**, **F**). No samples were recovered at 20 hours in summer and 32 hours in autumn and at the reference station in autumn due to bad weather. Summer reference station is located 35 km NNW from Darci's site and had a 3-fold lower abundance or MOB compared to Darci's site.

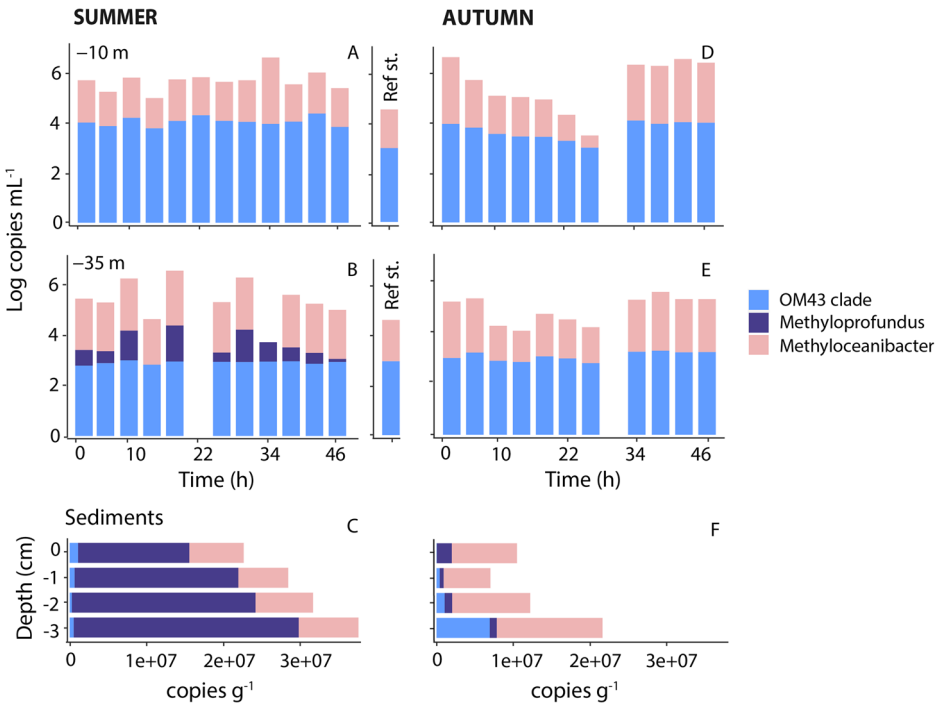

small because MOB consumes a substantial fraction of CH_4 in the water column. Nevertheless, temporal dynamics of seep activity and the strength and efficiency of the microbial CH_4 filter in the water column are scarcely constrained, because temporally replicated measurements on time scales of days and seasons are rarely conducted. With our sampling scheme, we were able to overcome these limitations. We repeatedly sampled at one location above an active seep, a point source injecting CH_4 into the water column where it was partly consumed by microbes but also drifted away with (tidal) currents.

Tidal imprint on seep activity

Our results showed rapid fluctuations in pulse strength, representing the flux of methane from sediment to water column during episodic release events, as well as in water column CH_4 inventories within hours, irrespective of the season (Fig. 2, Supplementary Table 5). Temporal changes on time scales of days to months in cold seep activity and CH_4 emissions have been described previously from continental margin[42] as well as deep water systems[23,28], but also in terrestrial systems[43], and could be linked to different forcing factors. Cold seeps can become active or dormant over periods

ranging from years to geological epochs due to cycles of gas reservoir depletion and refilling, as, e.g., observed for some mud volcanoes[44]. Seasonal variations have also been found to affect gas emissions on time scales of months: at coastal CH_4 release sites, phytoplankton blooms were shown to trigger elevated methanogenesis[45] and warmer water temperatures in summertime led to increased CH_4 release[40]. On shorter time scales of hours to days, sudden drops in hydrostatic pressure triggered by, e.g., storms[20,46], swells[42], and tides[14,24] have been found to facilitate enhanced bubble release from the seafloor.

Our observations at the Doggerbank seep area revealed a ~12 h periodicity, mostly pronounced in summertime (Fig. 2). This periodicity matches the frequency and timing of local tides fairly well. Nevertheless, tidally induced changes in current direction potentially transporting CH_4 charged waters from neighbouring flare clusters are unlikely to have caused the higher CH_4 inventories at Darci's site at low tide. Flare clusters were found in a Westerly direction relative to Darci's site (Fig. 1), but at low/rising tide, when we found maxima in CH_4 concentrations, the general current direction in the wider sampling area was NorthWest[47,48] (Fig. 2K–N, Supplementary Video S1–6). Indeed, we found the lowest CH_4 concentrations during high tide slack water and/or when the current flows North-East, i.e., when Darci's site was roughly downstream relative to the other flare clusters. Changes in current direction lead to a vertical bending of bubble plumes[25,49]. Consequently, CH_4 concentration at a fixed position next to a plume would be high or low, depending on whether the plume is bending towards or away from the measurements position. Variations in bottom water CH_4 concentrations influenced by a dispersing plume effect[25] are, nevertheless, unlikely to explain our observations. We continuously monitored and if needed adjusted the ship's position above Darci's site so that the CTD was lowered at the position where we found the base of the flare cluster. Our results thus rather provide evidence that hydrostatic pressure changes induced by tides are a key modulator of seep activity. The tidal range during our study was ~0.6 m in summer and ~0.9 m in autumn translating to a difference in hydrostatic pressure at the seafloor of ~0.6–0.9 dbar, i.e., <2.25% of the hydrostatic pressure at 41 m water depth (~41 dbar). Investigations at deep water seeps offshore Vancouver Island (1250 m water depth)[23] and in the Arctic at the Vestnesa ridge (900–1330 m water depth[24]) provided evidence that CH_4 ebullition from the seafloor may be modulated by even lower relative changes in hydrostatic pressure of 0.03% (Vancouver Island) to 0.1% (Vestnesa ridge). Continental margins are known to be macro—mesotidal areas which translates to tidal ranges of >4 m (macrotidal) to 2–4 m (mesotidal)[50] (note that Darci's site is located close to an amphidromic point which explains the relatively low tidal range). Open oceans on the other hand are characterised by microtidal ranges (<2 m)[50]. At continental margins, the typically high tidal range combined with a relatively shallow water depth thus translates to strong variations in hydrostatic pressure. Additionally, tidal forcing on the solid geosphere, i.e. body tides[19], might have further effects on CH_4 release from the sea floor. Body tides can trigger earthquakes and the inflation and deflation of magma chambers[51] and may thus also influence CH_4 release from cold seep systems such as Darci's site, which is fuelled from a shallow gas reservoir at 600 m below the seabed[52,53].

Our data directly show that CH_4 dynamics at cold seeps can only be resolved through repetitive measurements. Nevertheless, sampling strategies during previous sea-going expeditions usually did not resolve tidal cycles, and it remains unclear if these previous investigations on CH_4 dynamics at seeps were conducted during high or low tide. Thus, depending on the tidal conditions at the time of sampling, the CH_4 flux measured in those studies might likely have been under- or overestimated. For our seep location, single point measurements of CH_4 concentrations taken at low or high tide, for example, would yield high or low CH_4 concentrations, respectively. This raises the question: how much temporal sampling/measurement replication is necessary to describe the system well? We investigated the quantitative importance of repetitive measurements for one easy-to-measure parameter: water column CH_4 concentration. For each CTD cast, we determined a weighted average of dissolved CH_4 concentration (together with water depth, this parameter determines the local CH_4 inventory at the time of sampling). This was typically high at low tide and low at high tide (Fig. 2). For the summertime sampling campaign, the standard error of the average weighted CH_4 concentration was relatively high (±22% of the mean, $n = 24$) attesting to the high temporal variability of the system. We compared this average with values from bootstrapping analysis ($n = 24$), which yielded a similar result (Supplementary Table 6). Reducing the number of samples to $n = 10$ already resulted in a substantially higher error (Bootstrap SE) of more than ±34% of the mean. In autumn, the variation of the weighted CH_4 concentration was much lower (standard error = ± 5% of the mean, $n = 22$). Unlike for summer, lowering the bootstrap resampling only increased the Bootstrap SE slightly to ±7% ($n = 10$). For a system such as the Doggerbank seep area, temporal replication of $n < 10$ might consequently be too low to adequately capture variations in CH_4 dynamics during summertime conditions. For well-mixed conditions during autumn, on the other hand, the same number in temporal replication will likely be sufficient.

Factors controlling methane oxidation

Temporal dynamics of MOx, just as seepage activity, showed generally highest MOx rates at low tide and a periodicity, which suggests a tidal imprint. To the best of our knowledge, such a pattern of microbial activity in the water column has not been found before. While the dependence of MOx on CH_4 availability has been reported for longer times scales[18], we observed considerable changes in MOx rates on time scales of hours. Interestingly, we also found instances of high MOx rates when CH_4 concentrations were comparably low. For example, in surface waters in summer (after 20 h, Fig. 2). Then, CH_4 concentrations approached 108 nM, and MOx was 2.4 nM d^{-1} at 10 m water depth. However, two hours later at the same depth, CH_4 concentrations were three-fold lower, while MOx was only reduced by 1/3rd. Such non-linear response of MOx to CH_4 concentrations has also been found at other seep locations[13].

Previous publications found enhanced MOx activity in the wake of rising bubbles that drag microbes from sediments and deeper water layers upward[13,25,54]. We visually observed bubbles breaking the sea surface at Doggerbank during both campaigns, and our qPCR measurements showed that MOBs were present in both, the water column and in sediments during both seasons. Elevated MOB numbers and/or increased cell-specific CH_4 oxidation rates stimulated by higher CH_4 availability would also explain the higher k during low tide at times of higher MOx. Together with our findings of elevated MOx in surface waters, this indicates that a bubble-mediated advective transport could play an important role in recruiting surface water MOBs from deeper water layers and/or surface sediments. This transport is apparently strong enough to overcome the pycnocline which otherwise segregates surface and bottom waters in summertime.

Our results also showed substantial differences between sediment and water column MOB community composition (already on the level of presence/absence). This indicates that sediments can only, to a limited degree, act as a source for the water column MOB community. It thus appears likely that, in addition to bubble-mediated transport from surface sediments, water column MOBs were transported along with the rotating tidal current towards Darci's site. In fact, at our reference station (35 km NNW of Darci's site), we found similar MOB communities than at Darci's site. These were 2-fold (surface water) and 3-fold (bottom waters) less abundant (Fig. 5) while CH_4 concentrations and MOx rates were respectively 74 times and 36 times lower compared to the seep location (Supplementary Table 7). It seems unlikely that the MOBs at the reference site originate from sediments or the lower water column at the reference site itself because of the limited CH_4 availability there. Instead, we argue that currents may have transported MOBs from seep locations toward the reference site. Like vertical transport, currents (e.g., tidal currents) can thus act as a transport vector spreading MOBs over long horizontal distances. Shelf seas, including the North Sea, feature many seeps[9]. Thus, it is likely that seep locations like Darci's site act as seeding sites and as steppingstones for organisms like MOBs that are

dependent on (reduced) compounds such as CH_4 that are upwelled at cold seeps.

In addition to CH_4, oxygen and nutrient availability[21] are prerequisites for methanotrophic activity, too, as are stable environmental conditions[8,9,13,14,27] and a high standing stock of MOBs[9]. CH_4, oxygen, and nutrient availability are high at continental shelf seeps. The continuity of environmental conditions, which increases the residence time of a water mass above a cold seep, is primarily found during calm weather conditions when the water column is stratified. The prolonged exposure time of the water column MOB community to elevated CH_4 during the summer season triggers MOB activity and likely community growth, too, before the MOBs are translocated by currents. Ultimately, this establishes a more efficient microbial CH_4 filter[9]. In contrast, well-mixed conditions, often associated with frequent storms, result in more rapid dispersal of Methanotrophs away from high CH_4 conditions.

We only found a low diversity and low overall abundance of known type I methanotrophs within the water column, and we could not find apparent changes in diversity related to tidal dynamics (Fig. 4). This contrasts the rather high difference in water column MOx and suggests the presence of an undetected, or larger-than-detected, pelagic MOB community. It is thus likely that the currently available primers are not sufficient to cover the diversity of methanotrophs, at least in the marine realm[15,55]. In addition to canonical MOBs, we also found members of the Methyloceanibacter (family Methyloligellaceae). This genus has been found previously in North Sea sediments and was described as a methylotroph able to metabolise C_1-compounds other than CH_4. However, some Methyloceanibacter species contain a soluble methane monooxygenase (sMMO), suggesting that these organisms are able to directly oxidise CH_4, similar to a type II methanotroph[36]. Furthermore, other methylotrophic families, such as Methylophilaceae, were more abundant throughout water column and may be trophically associated with methanotrophs[37].

Fate of methane above Darci's site

The shallow gas reservoir fuelling the seep system to which also Darci's site belongs is located at ~600 m below the seabed[52,53] and hence not affected by seasonal variations in organic matter deposition[21,45], and temperature[28]. Without considering tidally induced variations, the overall seepage activity at the Doggerbank seep is thus likely constant throughout the year and independent of seasonal effects. Furthermore, previous water column CH_4 concentration measurements at the Doggerbank seep area in summer[29] were comparable to our findings, suggesting that seepage activity has been stable on time scales of at least years to decades. The strong difference in the average water column CH_4 inventory in summer versus autumn (4817 vs 2267 μmol m^{-2}, Table 1) is hence related to water column stratification. The pycnocline in summer acts as a physical barrier for dissolved CH_4[56–58] but also for microbes, including MOBs[13]. Summertime bottom waters comprise residual winter waters that are trapped below the pycnocline. Physically separated from surface waters, bottom waters then become supercharged with CH_4, and thus provide conditions of continuity for MOBs to thrive. In fact, MOx inventories showed that ~4 times more CH_4 was turned over in summer compared to autumn.

MOx discriminates against isotopically heavy CH_4 and thus causes an isotopic enrichment of residual CH_4. The modelled apparent isotope enrichment factors ε (Fig. 3 and Supplementary Fig. 5) are in agreement with literature values for microbial oxidation of CH_4 under oxic conditions in the ocean, but in particular for ε_H, this is lower than isotope enrichment factors determined from MOB cultures[59]. During summer, isotopically heavier CH_4 was observed at lower concentrations above the Rayleigh line, indicating that MOx activity contributed to a heavier isotopic signature. Nevertheless, the isotopic overprint is not only caused by MOx at Darci's site alone because isotopic signatures of CH_4 trace biogeochemical processes across spatial and temporal scales[60]. The isotopic signals at Darci's site during times of low seepage activity will likely integrate signals from the CH_4 source and ongoing MOx at Darci's site itself, but also a legacy signal from CH_4 transported by (tidal)currents towards Darci's site. This legacy CH_4 may likely have been isotopically overprinted by MOx, too. At times of higher seepage, Rayleigh fractionation processes were overprinted by the rapid influx of isotopically depleted CH_4 from the sea floor.

In autumn, deep mixing disturbs this continuity so that MOx becomes overall lower and mixing also leads to accelerated outgassing of CH_4 to the atmosphere. Stronger mixing in autumn was also evident from isotopically heavy CH_4, that, unlike isotopically heavy CH_4 in summertime, plots on (or close to) the mixing line of our endmember mixing model. The isotopically heavy values were thus more dominantly caused by admixture of atmospheric CH_4, which is enriched in ^{13}C and D compared to the microbial source signal at the Doggerbank seep area (Table 1)[53,61].

Sea–air flux of methane to the atmosphere

Bubbles rising from the ocean floor can transport substantial amounts of CH_4 to the sea surface and potentially to the atmosphere[11,49,62]. In fact, during high seepage activity at low tide, we found an isotopic source signal of seep CH_4 (i.e., about −80‰ for $\delta^{13}C$ and −185‰ for δD) throughout the water column. This suggests an effective vertical transport of CH_4 before it becomes consumed and isotopically overprinted by MOBs. Furthermore, we directly observed bubbles breaking the sea surface. In autumn, we measured the radii of these bubbles (up to 1.75 mm, Supplementary Fig. 3). These bubbles constantly exchange CH_4 (and other gases) with the surrounding water during their ascend from 41 m water depth. CH_4 bubbles rising through the water column were found to shrink because of bubble dissolution[63], but the strong relative change in pressure towards the sea surface also leads to an expansion of the bubble volume. i.e., a 1.75 mm bubble at the surface would have been compressed to ~1 mm at 40 m depth. Disregarding expansion, a pure CH_4 bubble of 1.75 mm size released from the sea floor will exchange most, but not all CH_4 with the adjacent sea water, i.e., it will contain $\lesssim$2.5% of the initial CH_4 load when reaching the sea surface[64]. Hence, though gas exchange and volumetric dissolution decelerate advective CH_4 flux, rising bubble transport will cause direct CH_4 release to the atmosphere at the Doggerbank seep.

Higher levels of dissolved CH_4 in well-mixed surface waters also increase diffusive efflux of CH_4 to the atmosphere. Our diffusive flux estimates were high, in particular in autumn (Table 1), and are very similar to CH_4 efflux values reported from a near shore shallow coastal area[40]. Previously estimated diffusive fluxes of 9 μmol m^{-2} d^{-1} in summer and 104 μmol m^{-2} d^{-1} in winter at the Doggerbank seep area[29] are ~7-fold lower than our observations for summer (64 μmol m^{-2} d^{-1}) and ~2-fold lower for autumn (180 μmol m^{-2} d^{-1}), respectively. Other sea surface-atmosphere flux estimates for the Doggerbank seep area (based on bubble flux modelling and backscatter data from spring 2016) were 458 μmol m^{-2} d^{-1} [23]. This flux estimate is based on an average bubble radius of 3 mm, which is $\gtrsim$2-fold higher than the larger bubble radii measured here. In addition, we argue that the differences in flux measurements are, at least in parts, related to the higher temporal resolution of the sampling applied here, which better averages between phases of high/low seepage caused by tides.

The lower efflux of CH_4 to the atmosphere in summer is caused by the presence of a stratification barrier slowing down advective and diffusive gas transport from bottom to well-mixed surface waters. Together with the overall higher MOx in summer, this mitigates outgassing of CH_4 to the atmosphere more effectively when compared to fully mixed autumn conditions with a high supply of CH_4 but low MOx activity. Finally, wind velocities in autumn are higher, which further accelerates CH_4 efflux. Our comparison of summer and autumn data shows the importance of conducting measurement campaigns in fair and rough weather conditions to avoid over-underestimation of the amount CH_4 liberated to the atmosphere.

Methane budget

The water column in the region of the Doggerbank seeps site is annually stratified for ~5 months between April and October)[65], and exhibits large interannual variability in the duration of the stratified period[66]. Wind speeds during these months are 7.9 m s^{-1} on average[66], while higher wind speeds of 9.5 m s^{-1} are encountered during the remaining 7 months of well-mixed

conditions. Average surface water CH_4 concentrations were 26 nM (this study) to 33 nM[29] during stratified conditions and 14 nM[29] to 33 nM (this study) at times of a fully mixed water column. Hence this translates to a diffusive annual CH_4 flux to the atmosphere of 12–16 mmol m^{-2} during stratified conditions and 10–26 mmol m^{-2} during mixed conditions (note that this does not account for bubble-mediated advective transport). These efflux values are comparable to observations from seeps in shallow waters at the Belgium shore[40] and on the Arctic shelf[67].

Materials and methods

Site description and sampling

The Doggerbank seep area is located within the Dutch sector of the North Sea (Fig. 1). During cruises PE-439 (June 2018) and PE-462 (October 2019) with R/V Pelagia, we monitored seep activity related oceanographical, physicochemical and biogeochemical parameters at a cluster of point sources where CH_4 is released to the water column (Darci's site: 55°18.371 N, 04°05.353 E; 41 m water depth). In the wider seep area, several active CH_4 point sources have been found previously[29,30]. Methane at the Doggerbank seep originates from shallow gas pockets located >600 m below seafloor[52,53]. Previous work found that uprising gas comprises CH_4 of a microbial origin with δ^{13}C-CH_4 values ranging between -62‰ and -71‰[53].

At Darci's site, we recovered discrete water samples every two hours (the sampling time series started at 13:30 h on date 29 June 2018 and at 11:30 h on date 12 October 2019). For this, the ship was kept stationary at location, and we checked that the relative position of the ship's crane was over the continuous active cold seep cluster using the ship's multibeam system (30 kHz Kongsberg EM302). Sampling was carried out with a rosette sampler with 24 × 12 L Niskin bottles. Water mass properties (temperature, salinity, density, oxygen) were measured continuously with a Sea-Bird (SBE911) + conductivity–temperature–depth (CTD) system. In summer, discrete water samples were recovered from 8 depths (2 m, 10 m, 15 m, 20 m, 25 m, 30 m, 35 m, and 40 m) and, upon recovery, immediately sampled for subsequent analyses of water column constituents. In late autumn, heavier weather conditions did not allow sampling between 29—34 hours of the time series, and at 40 m depth, so discrete water samples were recovered from 2 m, 5 m, 10 m, 15 m, 20 m, 25 m, 30 m, and 35 m water depth. Particulate organic matter (POM) was sampled every 4 hours at 10 m depth and 35 m depth using two McLane in situ pumps (WTS-LV) equiped with glass fibre filters (142 mm, 0.3 µm nominal mesh size, Advantec MFS). Per season, two sediment cores (15 and 18 cm in summer and 16 and 20 cm in autumn) were sampled with a multicorer device at rising tide in summer and high tide in autumn. The cores were consecutively sliced in a cold rooom (5 °C) in sections of 1 cm and stored at −20 °C until further analysis. Reference stations were located at 35 km NNW of Darci's site in summer (55° 36.492 N, 3° 57.352 E, 35 m depth) and 176 km SSE in autumn (53° 46.338 N, 4° 46.078 E, 35 m depth). Because of unfavourable sea conditions, in situ pumps for POM sampling could not be deployed at the reference station in autumn.

Dissolved CH_4 concentrations and stable isotope ratios

Dissolved CH_4 concentrations were determined using a headspace (HS) technique[68]. Briefly, 100 mL vials were filled HS-free with seawater and crimp top-sealed immediately after CTD recovery. Then, an HS was added by injection N_2 gas, and the sample was fixed with NaOH. CH_4 concentrations were measured by gas chromatography with flame ionisation detection[69] in our home laboratories. Inventories of CH_4 and MOx were computed by integrating values over a depth of 40 m in both seasons. Although each measurement offers a momentary snapshot, calculating CH_4 inventories is valuable for comparative analysis. It's important to note, however, that these values may not necessarily be representative of a broader geographic area. Similarly, seawater aliquots were sampled for CH_4 stable carbon and hydrogen isotope measurements. These samples were fixed with 100 µl $HgCl_2$ (2.5 mM). Isotope measurements were conducted according to previous publications[70,71]. Stable carbon and hydrogen isotope compositions are presented in the delta notation against VPDB and VSMOW, respectively, and have an analytical error of 0.05‰ (δ^{13}C) and 1.1‰ (δD). In autumn, δD-CH_4 values were not measured from all CH_4 samples during the first 24 h of the measurement series. Hence these values were not used for spatiotemporal analysis but, together with δ^{13}C-CH_4, for the endmember isotope mixing model.

Methane oxidation rate measurements

MOx was determined by ex-situ incubations with trace amounts of ^{3}H-labelled CH_4 as described previously[72]. Briefly, aliquots from each Niskin bottle were filled HS-free in 20 mL glass vials in triplicate, sealed with grey-bromobutyl stoppers that are known to not hamper methanotrophic activity[72] and amended with 5 µL of ^{3}H-CH_4/N_2 (4.5 kBq, American Radiolabeled Chemicals, USA). Samples were incubated for 72 h in the dark at in situ temperature. Activities of residual C^3H_4 and the MOx product ^3H_2O were measured by liquid scintillation counting.

First order rate constants (k) were determined from fractional tracer turnover[6]:

$$k = \frac{^3H_2O}{^3H_2O + C^3H_4} \times \frac{1}{2} \quad (2)$$

where t is incubation time in days. k was corrected for (negligible) tracer turnover in killed controls (KC, fixed with 100 µl $HgCl_2$ directly after sampling) and multiplied with CH_4 concentrations [CH_4], yielding MOx:

$$MO_X = (k - k_{KC}) \times [CH_4] \quad (3)$$

Diffusive fluxes of methane

Sea–air fluxes were calculated based on a boundary layer model that considers the relation between wind, temperature and CH_4 concentrations in the atmosphere and the well-mixed surface water layer[73]:

$$F = (pCH_{4w} - pCH_{4a})K_0 k_{CH_4} \quad (4)$$

where F denotes the diffusive CH_4 flux, pCH_{4w} and pCH_{4a} (in atm) are the partial pressures of CH_4 in the air and in the well-mixed surface water layer, respectively. pCH_{4a} was measured with a Picarro G2301 gas concentration analyser on board. pCH_{4w} was determined from surface water CH_4 concentrations (see above). K_0 is the CH_4 solubility in mol m^{-3} atm^{-1} [74] and was calculated from temperature and salinity obtained from corresponding CTD casts. k_{ch4} is the CH_4 gas transfer velocity in m d^{-1}, which was calculated using wind speed (U), the Schmidt number (Sc_{CH4}), and the normalised gas transfer velocity (k_{660}) according to ref. 73:

$$k_{CH_4} = 0.251\, U^2 \left(\frac{S_{c_{CH_4}}}{660}\right)^{-0.5} \quad (5)$$

Wind speed was measured on board at 10 m above sea level. The Schmidt number describes the ratio between kinematic viscosity of water and the gas diffusion coefficient, which relates the different k-values for different gases[73,75].

DNA extraction and 16S rRNA gene amplicon library preparation

DNA was extracted from particulate organic matter collected on filters and sediment core tops using the PowerSoil Pro DNA extraction kit (Mo Bio Laboratories, Carlsbad, CA, USA). DNA extracts were stored at −20 °C until further analysis. Gene amplification was performed in triplicate with the universal SSU primer pair 515F-Y/926 R targeting the V4 and V5 hypervariable regions and conducted as described earlier[76] but with an adaption to the PCR programme: 5 minutes initial enzyme activation/DNA denaturation at 98 °C, followed by 25 cycles of 98 °C for 1 minute, 58 °C for 1 minute, 72 °C for 2 minutes, with a final elongation of 72 °C for 10 min; after completion samples were stored at 5 °C. The 16S rRNA products

(~400 bp including unique Golay barcodes on forward and reverse primers) were gel purified, and further library preparation, pooling, and Illumina MiSeq 2 × 300 sequencing was done as described previously[76].

16S rRNA gene amplicon sequences were analysed using the NIOZ in-house Cascabel pipeline[76,77]. Prior to ASV identification, reads were truncated to 260 bp and 200 bp for forward and reverse reads, respectively. ASV designation was done using DADA2 v.1.19.1[78]. Identification by consensus across samples was used to identify chimeras, and sequence variants identified as chimeric were removed. Taxonomies were assigned using DADA2's native implementation of the naïve Bayesian classifier method RDP by using the Silva v138.1 release as reference database. Singletons with an abundance lower than 2, were excluded from further analyses, leaving 8110 ASVs for downstream analyses. Sequencing analysis and the commands used her are detailed in supplementary information.

Quantitative PCR methanotrophs

Specific PCR primers were designed for Methyloceanibacter, Methyloprofundus, and the OM43 clade and were chosen based on their presence in water column and/or sediments. Representative methanotrophic sequences (52 ASVs) were extracted from the next generation sequencing data set and these sequences were added to the reference tree of the Silva NR SSU Ref database, release v138.1 using the ARB Parsimony tool in the ARB software package[79]. Subsequently, specific primers for selected bacteria were designed using the Design Probes tool in ARB. Results were evaluated based on the following criteria: a maximum of two mismatches, not occurring in the last six bases at 3' side, were accepted in the target sequence; similarly, non-target sequences needed to have at least two mismatches to the primer of which at least one was at the final base at the 3' side. The newly designed primers (Supplementary Table 8) were tested on DNA extracts (2 ng μL^{-1}) of seven methylotrophic and methanotrophic cultures, namely Methylocystis rosea (DSM 17261), Methylosinus sporium (DSM 17706), Methylomonas methanica (DSM 25384), Methyloprofundus sedimenti (DSM 29215), Methylocaldum marinum (27392), Methyloceanibacter caenitepedi (DSM 27242), Methylophilus methylotrophus (DSM 5691), and gradient qPCRs were performed to determine the optimal selective annealing temperature.

qPCRs were carried out using a Accustart II PCR ToughMix (2×) (Quanta Biosciences). According to manufacturer's recommendations, the master mixture (20 µL) contained 10 µL Accustart II PCR toughmix 2×, 0.6 µL of each appropriate primer, 0.5 µL EvaGreen 20× qPCR dye, 7.3 µL ultrapure sterile water and 1 µL template DNA. A Bio-rad CFX96 Thermal cycler was used to run the qPCRs. The cycling conditions for the qPCR reactions consisted of an initial 3 min denaturation step at 94 °C, followed by 41 cycles of 30 sec denaturation at 98 °C, 15 sec annealing at 65 °C (Methyloceanibacter and OM43 clade primers) and 68 °C in case of Methyloprofundus, and a 1 min extension at 72 °C, followed by 5 min 72 °C and cooling step for 5 min at 4 °C. qPCR efficiency for Methyloceanibacter was 100.6% ($R^2 = 0.995$) in summer and 93.7% ($R^2 = 0.997$) in autumn. qPCR efficiency for Methyloprofundus was 100.8% ($R^2 = 0.984$) in summer and 76.7% ($R^2 = 0.989$) in autumn. qPCR efficiency for OM43 clade was 91.5% ($R^2 = 0.998$) in summer and 92.5% ($R^2 = 0.997$) in autumn.

Hydrodynamic modelling

Current fields were extracted from a pre-existing simulation of the North-west European Shelf with the well-established hydrodynamic model GETM (General Estuarine Transport Model[80], available at www.getm.eu). This simulation[48], with a spatial resolution of 0.08° × 0.05° (lon x lat, ~5 km), uses a Cartesian grid with 25 layers in the vertical (σ layers with enhanced vertical resolution at both the surface and seabed). The internal time step of the simulation was 10 seconds.

Surface and bottom current data were extracted at hourly intervals, allowing for a robust comparison with the observational data presented in this study. Three different spatial areas were extracted from the simulation: the "Methane Area" provides current visualisation around Darci's site (every model grid point shown), while the "Dogger Bank" area presents the circulation around the entire Dogger Bank (every third model point shown). Similarly, the "North Sea" extraction exhibits currents at a southern North Sea scale (every fifth grid point shown). Together, these selected areas provide a comprehensive evaluation of the hydrodynamic patterns on a local and regional scale that affect Darci's site. Temporal current visualisation at Darci's site was extracted from the closest model grid point (4.10°E, 55.30°N) to the observational location (4.09°E, 55.31°N). Simulated sea surface height was extracted at the same model location.

Conclusions

Our study provides evidence that tides strongly modulate the activity of cold seeps on continental shelves with an increase in CH_4 release from the sea floor during low tide. Higher seepage activity triggers elevated rates of microbial CH_4 oxidation, most importantly during warmer seasons because CH_4 and MOBs are retained in bottom waters during stratified conditions. In contrast, deep mixing during cold seasons accelerates liberation of CH_4 to the atmosphere and reduces MOx due to a lack of continuity. Our findings highlight the necessity of repeated sampling at hourly intervals and with repetitions throughout the year to resolve the temporal dynamics of seepage, methanotrophic activity, and sea–air fluxes of CH_4. Cold seeps are widespread at continental margins, but high-frequency sampling strategies allowing to resolve tidal cyclicity are usually not applied. Additionally, measurement campaigns are often conducted during fair weather conditions when most shelf seas feature water column stratification. We, therefore, argue that tidal oscillation and water column mixing regimes are underappreciated in global budget estimates of CH_4 efflux from shelf seas.

Data availability

All data will be archived and made publicly available in the DAS database (Data Archive System, https://doi.org/10.25850/nioz/7b.b.jh. Sequence data for this study have been deposited in the European Nucleotide Archive (ENA) at EMBL-EBI under accession number PRJEB76184.

Received: 2 June 2023; Accepted: 31 May 2024;
Published online: 12 July 2024

References

1. Etminan, M., Myhre, G., Highwood, E. J. & Shine, K. P. Radiative forcing of carbon dioxide, methane, and nitrous oxide: a significant revision of the methane radiative forcing. *Geophys. Res. Lett.* **43**, 12,614–612,623 (2016).
2. Masson-Delmotte et al. IPCC, 2021: Climate Change 2021: The Physical Science Basis. Contribution of working group i to the sixth assessment report of the intergovernmental panel on climate change. *In press* edn., (Cambridge University press, 2021).
3. Nisbet, E. G. et al. Very Strong Atmospheric Methane Growth in the 4 Years 2014–2017: Implications for the Paris Agreement. *Glob. Biogeochem. Cycles* **33**, 318–342 (2019).
4. Saunois, M. et al. The Global Methane Budget 2000–2017. *Earth Syst. Sci. Data* **12**, 1561–1623 (2020).
5. Weber, T., Wiseman, N. A. & Kock, A. Global ocean methane emissions dominated by shallow coastal waters. *Nat. Commun.* **10**, 4584 (2019).
6. Reeburgh, W. S. Oceanic methane biogeochemistry. *Chem. Rev.* **107**, 486–513 (2007).
7. Boetius, A. & Wenzhöfer, F. Seafloor oxygen consumption fuelled by methane from cold seeps. *Nat. Geosci.* **6**, 725–734 (2013).
8. James, R. H. et al. Effects of climate change on methane emissions from seafloor sediments in the Arctic Ocean: a review. *Limnol. Oceanogr.* **61**, S283–S299 (2016).
9. Steinle, L. et al. Water column methanotrophy controlled by a rapid oceanographic switch. *Nat. Geosci.* **8**, 378–382 (2015).
10. Suess, E. In *Hydrocarbons, oils and lipids: diversity, origin, chemistry and fate* (ed. Heinz Wilkes) 747–767 (Springer International Publishing, 2020).

11. McGinnis, D. F., Greinert, J., Artemov, Y., Beaubien, S. E. & Wüest, A. Fate of rising methane bubbles in stratified waters: how much methane reaches the atmosphere? *J. Geophys. Res.* **111**, https://doi.org/10.1029/2005jc003183 (2006).
12. Schneider von Deimling, J. et al. Quantification of seep-related methane gas emissions at Tommeliten, North Sea. *Cont. Shelf Res.* **31**, 867–878 (2011).
13. Steinle, L. et al. Linked sediment and water-column methanotrophy at a man-made gas blowout in the North Sea: implications for methane budgeting in seasonally stratified shallow seas. *Limnol. Oceanogr.* **61**, S367–S386 (2016).
14. Gründger, F. et al. Seasonal shifts of microbial methane oxidation in Arctic shelf waters above gas seeps. *Limnol. Oceanogr.* **66**, 1896–1914 (2021).
15. Knief, C. Diversity and habitat preferences of cultivated and uncultivated aerobic methanotrophic bacteria evaluated based on pmoA as molecular marker. *Front. Microbiol.* **6**, 1346 (2015).
16. Whiticar, M. J. Carbon and hydrogen isotope systematics of bacterial formation and oxidation of methane. *Chem. Geol.* **161**, 291–314 (1999).
17. Barker, J. F. & Fritz, P. Carbon isotope fractionation during microbial methane oxidation. *Nature* **293**, 289–291 (1981).
18. Crespo-Medina, M. et al. The rise and fall of methanotrophy following a deepwater oil-well blowout. *Nat. Geosci.* **7**, 423–427 (2014).
19. Lau, H. C. P. & Schindelegger, M. In *A Journey Through Tides* (eds Mattias G. & João C. D.) 365–387 (Elsevier, 2023).
20. Lohrberg, A. et al. Discovery and quantification of a widespread methane ebullition event in a coastal inlet (Baltic Sea) using a novel sonar strategy. *Sci. Rep.* **10**, 4393 (2020).
21. Steinle, L. et al. Effects of low oxygen concentrations on aerobic methane oxidation in seasonally hypoxic coastal waters. *Biogeosciences* **14**, 1631–1645 (2017).
22. de Groot, T. R. et al. Diel and seasonal methane dynamics in the shallow and turbulent Wadden Sea. *Biogeosciences* **20**, 3857–3872 (2023).
23. Römer, M., Riedel, M., Scherwath, M., Heesemann, M. & Spence, G. D. Tidally controlled gas bubble emissions: a comprehensive study using long-term monitoring data from the NEPTUNE cabled observatory offshore Vancouver Island. *Geochem. Geophys. Geosyst.* **17**, 3797–3814 (2016).
24. Sultan, N., Plaza-Faverola, A., Vadakkepuliyambatta, S., Buenz, S. & Knies, J. Impact of tides and sea-level on deep-sea Arctic methane emissions. *Nat. Commun.* **11**, 5087 (2020).
25. Jordan, S. F. A. et al. Pelagic methane sink enhanced by benthic methanotrophs ejected from a gas seep. *Geophys. Res. Lett.* **48**, e2021GL094819 (2021).
26. Boles, J. R., Clark, J. F., Leifer, I. & Washburn, L. Temporal variation in natural methane seep rate due to tides, Coal Oil Point area, California. *J. Geophys. Res. Oceans* **106**, 27077–27086 (2001).
27. Mau, S., Blees, J., Helmke, E., Niemann, H. & Damm, E. Vertical distribution of methane oxidation and methanotrophic response to elevated methane concentrations in stratified waters of the Arctic fjord Storfjorden (Svalbard, Norway). *Biogeosciences* **10**, 6267–6278 (2013).
28. Ferré, B. et al. Reduced methane seepage from Arctic sediments during cold bottom-water conditions. *Nat. Geosci.* **13**, 144–148 (2020).
29. Mau, S. et al. Seasonal methane accumulation and release from a gas emission site in the central North Sea. *Biogeosciences* **12**, 5261–5276 (2015).
30. Römer, M. et al. Assessing marine gas emission activity and contribution to the atmospheric methane inventory: a multidisciplinary approach from the Dutch Dogger Bank seep area (North Sea). *Geochem. Geophys. Geosyst.* **18**, 2617–2633 (2017).
31. Czerski, H. et al. Ocean bubbles under high wind conditions—Part 1: bubble distribution and development. *Ocean Sci.* **18**, 565–586 (2022).
32. Milkov, A. V. & Etiope, G. Revised genetic diagrams for natural gases based on a global dataset of >20,000 samples. *Org. Geochem.* **125**, 109–120 (2018).
33. Jacques, C. et al. Carbon and hydrogen isotope signatures of dissolved methane in the Scheldt Estuary. *Estuaries Coasts* **44**, 137–146 (2021).
34. Mariotti, A. et al. Experimental determination of nitrogen kinetic isotope fractionation: some principles; illustration for the denitrification and nitrification processes. *Plant Soil* **62**, 413–430 (1981).
35. Quay, P. et al. The isotopic composition of atmospheric methane. *Glob. Biogeochem. Cycles* **13**, 445–461 (1999).
36. Vekeman, B. et al. New Methyloceanibacter diversity from North Sea sediments includes methanotroph containing solely the soluble methane monooxygenase. *Environ. Microbiol.* **18**, 4523–4536 (2016).
37. Taubert, M. et al. Communal metabolism by Methylococcaceae and Methylophilaceae is driving rapid aerobic methane oxidation in sediments of a shallow seep near Elba, Italy. *Environ. Microbiol.* **21**, 3780–3795 (2019).
38. Takeuchi, M. et al. Correction: possible cross-feeding pathway of facultative methylotroph methyloceanibacter caenitepidi Gela4 on methanotroph Methylocaldum marinum S8. *PLoS One* **16**, e0251538 (2021).
39. van Grinsven, S., Sinninghe Damsté, J. S., Harrison, J., Polerecky, L. & Villanueva, L. Nitrate promotes the transfer of methane-derived carbon from the methanotroph Methylobacter sp. to the methylotroph Methylotenera sp. in eutrophic lake water. *Limnol. Oceanogr.* **66**, 878–891 (2021).
40. Borges, A. V., Champenois, W., Gypens, N., Delille, B. & Harlay, J. Massive marine methane emissions from near-shore shallow coastal areas. *Sci. Rep.* **6**, 27908 (2016).
41. Shakhova, N. et al. Extensive methane venting to the atmosphere from sediments of the East Siberian Arctic shelf. *Science* **327**, 1246–1250 (2010).
42. Leifer, I. Turbine tent measurements of marine hydrocarbon seeps on subhourly timescales. *J. Geophys. Res.* **110**, https://doi.org/10.1029/2003jc002207 (2005).
43. Etiope, G., Feyzullayev, A. & Baciu, C. L. Terrestrial methane seeps and mud volcanoes: a global perspective of gas origin. *Mar. Pet. Geol.* **26**, 333–344 (2009).
44. Niemann, H. In *Hydrocarbons, oils and lipids: diversity, origin, chemistry and fate* (eds. Heinz W.) 769–780 (Springer International Publishing, 2020).
45. Bange, H. W. et al. Dissolved methane during hypoxic events at the Boknis Eck time series station (Eckernförde Bay, SW Baltic Sea). *Biogeosciences* **7**, 1279–1284 (2010).
46. Shakhova, N. et al. Ebullition and storm-induced methane release from the East Siberian Arctic Shelf. *Nat. Geosci.* **7**, 64–70 (2013).
47. ADMIRALTY Hydrographic Office. *NP253 - Admiralty Tidal Stream Atlas: North Sea - Eastern part*. (2004).
48. van der Molen, J., van Leeuwen, S. M., Govers, L. L., van der Heide, T. & Olff, H. Potential micro-plastics dispersal and accumulation in the North Sea, with application to the MSC Zoe incident. *Front. Mar. Sci.* **8**, https://doi.org/10.3389/fmars.2021.607203 (2021).
49. Schneider von Deimling, J., Linke, P., Schmidt, M. & Rehder, G. Ongoing methane discharge at well site 22/4b (North Sea) and discovery of a spiral vortex bubble plume motion. *Mar. Pet. Geol.* **68**, 718–730 (2015).
50. Gerkema, T. *An introduction to tides*. (Cambridge University Press, 2019).
51. Scholz, C. H., Tan, Y. J. & Albino, F. The mechanism of tidal triggering of earthquakes at mid-ocean ridges. *Nat. Commun.* **10**, 2526 (2019).
52. Schroot, B. M., Klaver, G. T. & Schüttenhelm, R. T. E. Surface and subsurface expressions of gas seepage to the seabed—examples from the Southern North Sea. *Mar. Pet. Geol.* **22**, 499–515 (2005).

53. Verweij, J. M. et al. Generation, migration, entrapment and leakage of microbial gas in the Dutch part of the Southern North Sea Delta. *Mar. Pet. Geol.* **97**, 493–516 (2018).
54. Jordan, S. F. A. et al. Bubble-mediated transport of benthic microorganisms into the water column: identification of methanotrophs and implication of seepage intensity on transport efficiency. *Sci. Rep.* **10**, 4682 (2020).
55. Tavormina, P. L., Orphan, V. J., Kalyuzhnaya, M. G., Jetten, M. S. & Klotz, M. G. A novel family of functional operons encoding methane/ammonia monooxygenase-related proteins in gammaproteobacterial methanotrophs. *Environ. Microbiol. Rep.* **3**, 91–100 (2011).
56. Gentz, T. et al. A water column study of methane around gas flares located at the West Spitsbergen continental margin. *Cont. Shelf Res.* **72**, 107–118 (2014).
57. Myhre, C. L. et al. Extensive release of methane from Arctic seabed west of Svalbard during summer 2014 does not influence the atmosphere. *Geophys. Res. Lett.* **43**, 4624–4631 (2016).
58. Schmale, O. et al. Bubble transport mechanism: indications for a gas bubble-mediated inoculation of benthic methanotrophs into the water column. *Cont. Shelf Res.* **103**, 70–78 (2015).
59. Kawagucci, S. et al. Hydrogen and carbon isotope fractionation factors of aerobic methane oxidation in deep-sea water. *Biogeosciences* **18**, 5351–5362 (2021).
60. Kessler, J. D., Reeburgh, W. S. & Tyler, S. C. Controls on methane concentration and stable isotope (δ2H-CH4 and δ13C-CH4) distributions in the water columns of the Black Sea and Cariaco Basin. *Glob. Biogeochem. Cycles* **20**, https://doi.org/10.1029/2005GB002571 (2006).
61. Lan, X., Nisbet, E. G., Dlugokencky, E. J. & Michel, S. E. What do we know about the global methane budget? Results from four decades of atmospheric CH4 observations and the way forward. *Philos. Trans. R. Soc. A* **379**, 20200440 (2021).
62. Veloso, M., Greinert, J., Mienert, J. & De Batist, M. A new methodology for quantifying bubble flow rates in deep water using splitbeam echosounders: examples from the Arctic offshore NW-Svalbard. *Limnol. Oceanogr. Methods* **13**, 267–287 (2015).
63. Rehder, G., Brewer, P. W., Peltzer, E. T. & Friederich, G. Enhanced lifetime of methane bubble streams within the deep ocean. *Geophys. Res. Lett.* **29**, 21–21 (2002).
64. Leifer, I. & Patro, R. K. The bubble mechanism for methane transport from the shallow sea bed to the surface: a review and sensitivity study. *Cont. Shelf Res.* **22**, 2409–2428 (2002).
65. Greenwood, N. et al. Detection of low bottom water oxygen concentrations in the North Sea; implications for monitoring and assessment of ecosystem health. *Biogeosciences* **7**, 1357–1373 (2010).
66. Karagali, I., Peña, A., Badger, M. & Hasager, C. B. Wind characteristics in the North and Baltic Seas from the QuikSCAT satellite. *Wind Energy* **17**, 123–140 (2014).
67. Thornton, B. F. et al. Shipborne eddy covariance observations of methane fluxes constrain Arctic sea emissions. *Sci. Adv.* **6**, 7934 (2020).
68. Green, J. D. In *Encyclopedia of Analytical Science (Second edition)* (eds Paul, W., Alan, T. & Colin P.) 229–236 (Elsevier, 2005).
69. Silyakova, A. et al. Physical controls of dynamics of methane venting from a shallow seep area west of Svalbard. *Cont. Shelf Res.* **194**, 104030 (2020).
70. Röckmann, T. et al. In situ observations of the isotopic composition of methane at the Cabauw tall tower site. *Atmos. Chem. Phys.* **16**, 10469–10487 (2016).
71. Menoud, M. et al. Characterisation of methane sources in Lutjewad, The Netherlands, using quasi-continuous isotopic composition measurements. *Tellus B: Chem. Phys. Meteorol.* **72**, 1–20 (2020).
72. Niemann, H. et al. Toxic effects of lab-grade butyl rubber stoppers on aerobic methane oxidation. *Limnol. Oceanogr.: Methods* **13**, 40–52 (2015).
73. Wanninkhof, R. Relationship between wind speed and gas exchange over the ocean revisited. *Limnol. Oceanogr.: Methods* **12**, 351–362 (2014).
74. Wiesenberg, D. A. & Guinasso, N. L. Equilibrium Solubilities of Methane, Carbon Monoxide, and Hydrogen in Water and Sea Water. *J. Chem. Eng. Data* **24**, 356–360 (1979).
75. Jähne, B. et al. On the parameters influencing air-water gas exchange. *J. Geophys. Res.: Oceans* **92**, 1937–1949 (1987).
76. Vaksmaa, A. et al. Microbial Communities on Plastic Polymers in the Mediterranean Sea. *Frontiers in Microbiology* **12**, https://doi.org/10.3389/fmicb.2021.673553 (2021).
77. Abdala Asbun, A. et al. Cascabel: a scalable and versatile amplicon sequence data analysis pipeline delivering reproducible and documented results. *Front. Genet.* **11**, https://doi.org/10.3389/fgene.2020.489357 (2020).
78. Callahan, B. J. et al. DADA2: high-resolution sample inference from Illumina amplicon data. *Nat. Methods* **13**, 581–583 (2016).
79. Ludwig, W. et al. ARB: a software environment for sequence data. *Nucleic Acids Res.* **32**, 1363–1371 (2004).
80. Burchard, H. & Bolding, K. K. GETM, a general estuarine transport model. (2002).

Acknowledgements

We thank our colleagues from the Royal Netherlands Institute for Sea Research (NIOZ), who provided insight and expertise that greatly assisted the research. We specifically thank Harry Witte for assistance with Cascabel, Sanne Vreugdenhil, and Maartje Brouwer for setting up the qPCR method, Emna Zeghal and Bart Meijninger, and the captain and crew of R/V Pelagia for their help at sea. We would also like to show our gratitude to Pierre Ramond and Julia Engelmann for their insights and help with sequence work.

Author contributions

The study was designed by Tim de Groot, Thomas Röckmann, and Helge Niemann. Tim de Groot, Victor Hernando-Morales, Sylvia Walter, and Helge Niemann performed the on-board sampling. Tim de Groot and Malika Menoud conducted the geochemical analysis. Tim de Groot measured the microbial rates. Darci Rush provided the coordinates for the seep location and helped with editing. Hossein Maazallahi conducted the atmospheric measurements and data processing. Helen Czerski performed the bubble measurements and data processing. Judith van Bleijswijk designed MOB primers and supervised the molecular analysis. Current modeling work was completed by Sonja van Leeuwen and Johan van der Molen, and the entire research project was supervised by Helge Niemann. The manuscript was prepared by Tim de Groot with input from all authors.

Competing interests

The authors declare no competing interests.

Additional information

Supplementary information The online version contains supplementary material available at https://doi.org/10.1038/s43247-024-01483-8.

Correspondence and requests for materials should be addressed to Tim R. de Groot or Helge Niemann.

Peer review information *Communications Earth & Environment* thanks Daniel McGinnis, Oliver Schmale, and the other, anonymous, reviewer(s) for their contribution to the peer review of this work. Primary Handling Editors: Erin Bertrand, Clare Davis, Alice Drinkwater and Aliénor Lavergne. A peer review file is available.